A fast algorithm for multiple elimination and transmission compensation in primary reflections

Zhang, Lele; Slob, Evert

A fast algorithm for multiple elimination and transmission compensation in primary reflections

Lele Zhang and Evert Slob

Delft University of Technology, 2628 CN Delft, The Netherlands. E-mail: L.Zhang-1@tudelft.nl

SUMMARY
The transmission compensated primary reflections can be obtained from the single-sided acoustic reflection response in the two-way traveltime domain. This is achieved by eliminating free-surface and internal multiple reflections and compensating for transmission losses in primary reflections without model information. The substantial computational cost of the proposed scheme can be reduced by an order of magnitude with a fast implementation version. This is achieved by using the previously computed filter functions as initial estimate for every new truncation time value. We evaluate the success of the scheme with simple and complex 2-D numerical examples. We find that the scheme has excellent performance in most cases, except for the case where strong reflectors are present. In such case, the current scheme suffers from lack of convergence.

Key words: Controlled source seismology; Wave scattering and diffraction.

INTRODUCTION

Many standard migration methods are based on the single-scattering assumption. This implies that all events in the measured data are treated as primary reflections. Besides primary reflections measured seismic data contain free-surface and internal multiple reflections. In standard migration methods, these multiple reflections are imaged as deeper artificial reflectors, which may lead to erroneous interpretation. Several schemes have been proposed to remove the artefacts arising from free-surface and internal multiple reflections. Some focus on free-surface and internal multiple elimination in data domain (Weglein *et al.* 1997; Zhang & Slob 2019), some attempt to use free-surface multiple reflections as useful signals to image the subsurface (Brown & Guitton 2005) or eliminate free-surface multiple reflection related artefacts in the imaging domain (Wang *et al.* 2014, 2017).

Free-surface multiple reflections can be very strong and cause major artefacts in the migrated image from marine seismic data. Much effort has been devoted to their removal in the data domain and several successful schemes have been developed. The surface-related multiple elimination (SRME) scheme (Verschuur *et al.* 1992) is a good example. SRME consists of two steps: free-surface multiple reflection prediction and subtraction. In the first step, free-surface multiple reflections are predicted by convolution of the traces in the measured data. Because the source wavelet is not known exactly, the amplitudes of predicted events differ from actual events in the measured data. Hence, adaptive subtraction is required to subtract the predicted multiple reflections from the measured data in the second step. The estimation of primaries by sparse inversion (EPSI, van Groenestijn & Verschuur 2009) replaces the two-step

processing of SRME by a full-waveform inversion process. Both the SRME and EPSI have achieved success for synthetic and field data sets (Lopez & Verschuur 2015).

Also internal multiple reflections cause artefacts in the migrated image from land and marine data and much effort has been devoted to their removal in the data domain. The inverse scattering series (ISS) based internal multiple reflection elimination scheme can make an approximate prediction of all orders of internal multiple reflections in one step without model information (Weglein *et al.* 1997; Ten Kroode 2002; Löer *et al.* 2016). Adaptive subtraction needs to be used to subtract the predicted internal multiple reflections from the measured data because of the approximate amplitude of predicted events (Matson *et al.* 1999; Luo *et al.* 2011; de Melo *et al.* 2014). Meles *et al.* (2015) combine the Marchenko scheme (Slob *et al.* 2014; Wapenaar *et al.* 2014) with convolutional interferometry to attenuate internal multiple reflections in measured data. However, model information and adaptive subtraction are required to apply this scheme.

Van der Neut & Wapenaar (2016) and Zhang *et al.* (2019) propose to eliminate internal multiple reflections from measured data without model information or adaptive subtraction. The transmission losses in primary reflections are compensated for in the scheme of Zhang *et al.* (2019). The performance of these schemes in 2-D numerical examples has been illustrated, but the application to field data has not been shown yet. Zhang & Slob (2019) extend the scheme of van der Neut & Wapenaar (2016) to account also for free-surface multiple reflections. In their scheme free-surface and internal multiple reflections are eliminated successfully in one step without requiring model information or adaptive subtraction.

In this paper, we propose two important modifications to the work of Zhang & Slob (2019). First, not only do we remove free-surface and internal multiple reflections, but also compensate for transmission losses in primary reflections by introducing the modified truncation window in Zhang *et al.* (2019). Secondly, we develop a fast implementation version that reduces the computational cost of the proposed scheme by an order of magnitude. The paper is organized as follows. In the theory section, we give the equations derived in Zhang & Slob (2019) with the truncations used in Zhang *et al.* (2019). We show how the proposed scheme can be implemented to reduce the computational cost significantly. In the numerical section, we apply this scheme to simple and complex 2-D numerical examples to evaluate the performance. The limitations of this scheme are explored in the limitations analysis section and we end with conclusions.

THEORY

We indicate time as t and a spatial location as $\mathbf{x} = (\mathbf{x}_H, z)$ with $\mathbf{x}_H = (x, y)$, where z denotes depth and $\mathbf{x}_H$ denotes the vector containing the horizontal coordinates. The pressure-free surface $\partial\mathbf{D}_0$ is defined at $z_0 = 0$. We express the acoustic impulse reflection response as $R(\mathbf{x}'_0, \mathbf{x}_0, t)$, where $\mathbf{x}'_0$ denotes the receiver position and $\mathbf{x}_0$ denotes the source position at the free surface $\partial\mathbf{D}_0$. The projected Marchenko equations in Zhang & Slob (2019) are given here with a modified truncation window in Zhang *et al.* (2019) to compensate for the transmission losses in primary reflections

$$v^-(\mathbf{x}'_0, \mathbf{x}''_0, t, t_2) = R(\mathbf{x}'_0, \mathbf{x}''_0, t) + \int_{\partial\mathbf{D}_0} d\mathbf{x}_0 \int_0^{+\infty} R(\mathbf{x}'_0, \mathbf{x}_0, t')$$
$$\times [v^+(\mathbf{x}_0, \mathbf{x}''_0, t-t', t_2) - r v^-(\mathbf{x}_0, \mathbf{x}''_0, t-t', t_2)] dt',$$
$$\text{for} \quad \varepsilon < t < t_2 + \varepsilon \tag{1}$$

$$v^+(\mathbf{x}'_0, \mathbf{x}''_0, t, t_2) = \int_{\partial\mathbf{D}_0} d\mathbf{x}_0 \int_{-\infty}^0 R(\mathbf{x}'_0, \mathbf{x}_0, -t')$$
$$\times [v^-(\mathbf{x}_0, \mathbf{x}''_0, t-t', t_2) - r v^+(\mathbf{x}_0, \mathbf{x}''_0, t-t', t_2)] dt',$$
$$\text{for} \quad \varepsilon < t < t_2 + \varepsilon, \tag{2}$$

where $v^\pm$ are the down- and upgoing filter functions as defined in Zhang *et al.* (2019), r indicates the reflection coefficient of the free surface, ε is a small positive value to account for the finite bandwidth, and t_2 denotes any desired time value within the time window of the measurement. Note that with the choice of the truncation window in eqs (1) and (2), the filter functions here are different from those in Zhang & Slob (2019). As explained in Zhang *et al.* (2019), the modified truncation window ensures to capture the desired primary reflection at t_2 in the filter function with transmission losses compensated. This transmission compensated primary reflection will be found at t_2 in case t_2 happens to be the two-way traveltime of a reflector, otherwise the value at t_2 will be zero, as shown in Fig. 1. Therefore, similar to Zhang *et al.* (2019), we can store the value of each v^- with two-way traveltime t_2 in a new data set. The new data set is free from free-surface and internal multiple reflections and contains only the corresponding transmission compensated primary reflections. It can be written as:

$$R_r(\mathbf{x}'_0, \mathbf{x}''_0, t = t_2) = v^-(\mathbf{x}'_0, \mathbf{x}''_0, t_2, t_2), \tag{3}$$

where R_r denotes the retrieved transmission compensated primary reflections.

Here we choose to solve eqs (1) and (2) iteratively as follows:

$$v_k^-(\mathbf{x}'_0, \mathbf{x}''_0, t, t_2) = R(\mathbf{x}'_0, \mathbf{x}''_0, t) + \int_{\partial\mathbf{D}_0} d\mathbf{x}_0 \int_0^{+\infty} R(\mathbf{x}'_0, \mathbf{x}_0, t')$$
$$\times [v_{k-1}^+(\mathbf{x}_0, \mathbf{x}''_0, t-t', t_2) - r v_{k-1}^-(\mathbf{x}_0, \mathbf{x}''_0, t-t', t_2)] dt',$$
$$\text{for} \quad \varepsilon < t < t_2 + \varepsilon \tag{4}$$

$$v_k^+(\mathbf{x}'_0, \mathbf{x}''_0, t, t_2) = \int_{\partial\mathbf{D}_0} d\mathbf{x}_0 \int_{-\infty}^0 R(\mathbf{x}'_0, \mathbf{x}_0, -t')$$
$$\times [v_k^-(\mathbf{x}_0, \mathbf{x}''_0, t-t', t_2) - r v_{k-1}^+(\mathbf{x}_0, \mathbf{x}''_0, t-t', t_2)] dt',$$
$$\text{for} \quad \varepsilon < t < t_2 + \varepsilon, \tag{5}$$

where $k = 1, 2, ...$ indicates the iteration number, and the choice

$$v_0^-(\mathbf{x}'_0, \mathbf{x}''_0, t, t_2) = 0, \tag{6}$$

$$v_0^+(\mathbf{x}'_0, \mathbf{x}''_0, t, t_2) = 0, \tag{7}$$

initializes the iterative scheme presented in eqs (4) and (5). Thus, eqs (1) and (2) can be solved iteratively for each value of t_2 with starting t_2 from zero to cover the whole recording time and incrementing t_2 with the time sampling dt of the data set.

We make an interesting observation from Fig. 1. In Fig. 1(a), the two-way traveltime associated with the horizontal dotted line is the time instant t_2. Suppose we have computed $v^\pm$ for t_2 and we would like to compute it now for a later time instant $t_2 + dt$, such that the new depth level with two-way traveltime $t_2 + dt$ is still above the third reflector. In that case the filter functions $v^\pm$ do not change and we have $v^\pm(\mathbf{x}'_0, \mathbf{x}''_0, t, t_2 + dt) = v^\pm(\mathbf{x}'_0, \mathbf{x}''_0, t, t_2)$. In Fig. 1(b), the value of $t_2 + dt$ leads to inclusion of the third reflector. Even then, all previously obtained filter values remain unchanged and new values that need to be computed are associated only with the third reflector. These new values can occur in the whole time window ($\varepsilon < t < t_2 + dt + \varepsilon$) of the filters. Thus, for a new time instant $t_2 + dt$, the initial estimate is given by

$$v_0^-(\mathbf{x}'_0, \mathbf{x}''_0, t, t_2 + dt) = v^-(\mathbf{x}'_0, \mathbf{x}''_0, t, t_2),$$
$$\text{for} \quad \varepsilon < t < t_2 + dt + \varepsilon \tag{8}$$

$$v_0^+(\mathbf{x}'_0, \mathbf{x}''_0, t, t_2 + dt) = v^+(\mathbf{x}'_0, \mathbf{x}''_0, t, t_2).$$
$$\text{for} \quad \varepsilon < t < t_2 + dt + \varepsilon. \tag{9}$$

As long as each new depth level, with two-way traveltime $t_2 + dt$, does not cross a new reflector, the iteration will terminate and we move to the next time instant. If the new depth level crosses a new reflector, $v_1^-(\mathbf{x}'_0, \mathbf{x}''_0, t, t_2 + dt)$ will be different from $v_0^-(\mathbf{x}'_0, \mathbf{x}''_0, t, t_2 + dt)$ and more iterations are required to properly account for the related events. Generally, fewer iterations are required than when the initial estimates given in eqs (6) and (7) are used for solving the iterative scheme presented in eqs (4) and (5). In 2-D or 3-D modelled data and in field data, every new time instant t_2 will possibly include a new (part of a) reflector. Still, fewer iterations are needed than with zero initial estimates, because all previously computed filter values will remain correct and only new ones related to the new reflector need to be computed. The retrieval of transmission compensated primary reflections from eq. (3) with the new initial estimates will reduce the computational cost compared with solving the equation with zero initial estimates for each time instant. Because the method retains its non-recursive character, the new implementation is different from layer-stripping schemes.
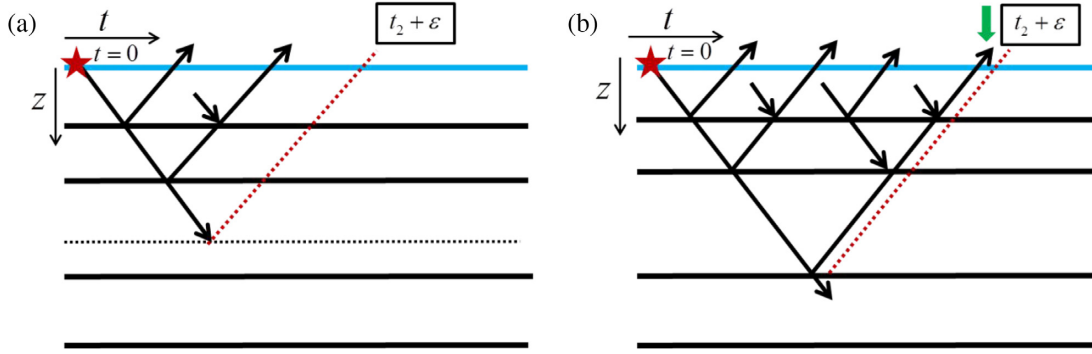
Figure 1. (a) 1-D sketch of the filter functions with focusing level far from reflectors; (b) 1-D sketch of the filter functions with focusing level coinciding with a reflector. The downgoing arrows indicate the downgoing filter function v^+ and the upgoing arrows indicate the upgoing filter function v^-. The black dotted horizontal line in (a) indicates the focusing level. In each plot, the red star indicates the source point and the red dotted line indicates the right boundary of the truncation window inside the subsurface, the green arrow in (b) indicates the event with two-way traveltime t_2. The blue solid line indicates the pressure-free surface.

Errors that are made at earlier traveltimes will be corrected at later traveltimes rather than be propagated and accumulated.

Compared with Zhang & Slob (2019) and Zhang *et al.* (2019), the retrieved data R_r from eq. (3) is not only free from free-surface and internal multiple reflections, the transmission losses in the primary reflections in R_r are also successfully compensated for. Moreover, the iterative solution in eqs (4) and (5) with the modified initial estimate given in eqs (8) and (9) is less computationally expensive as the number of iterations required to find the satisfied solutions for the subsequent filter functions is smaller than with the zero initial estimates given in eqs (6) and (7). No model information or adaptive filtering is required to run the scheme.

NUMERICAL EXAMPLES

In this section, two numerical examples are given to validate the effectiveness of our scheme for multiple reflection elimination and transmission losses compensation. In these two examples, the reflection responses are modelled with absorbing boundary conditions applied at the two sides and the bottom of models, and the top surface is set as a pressure-free surface, with the reflection coefficient of the free surface r given as –1 (note that the proposed scheme is valid for any choice of r). Sources and receivers are positioned at the free surface of each model and the spacing is 10 m. A Ricker wavelet with 20 Hz centre frequency is emitted by the sources. The direct wave has been removed from the modelled reflection responses. In this section, eqs (4) and (5) will be solved for each value of t_2 with starting t_2 from zero to cover the whole recording time and incrementing t_2 with the time sampling 0.004 s of the data set.

Horizontally layered model

Here, we consider a horizontally layered model to evaluate the scheme for removing multiple reflections and compensating for transmission losses in the primary reflections. Figs 2(a) and (b) show the acoustic velocity and density values of the model. We have modelled the reflection responses with 401 sources and 401 traces per shot gather, one of the modelled reflection responses is shown in Fig. 3(a). It can be seen that free-surface and internal multiple reflections are present as indicated by red arrows. The modelled reflection responses are used to solve eqs (4) and (5) for v^- in the fast fashion at each time instant t_2. The satisfied v^- can
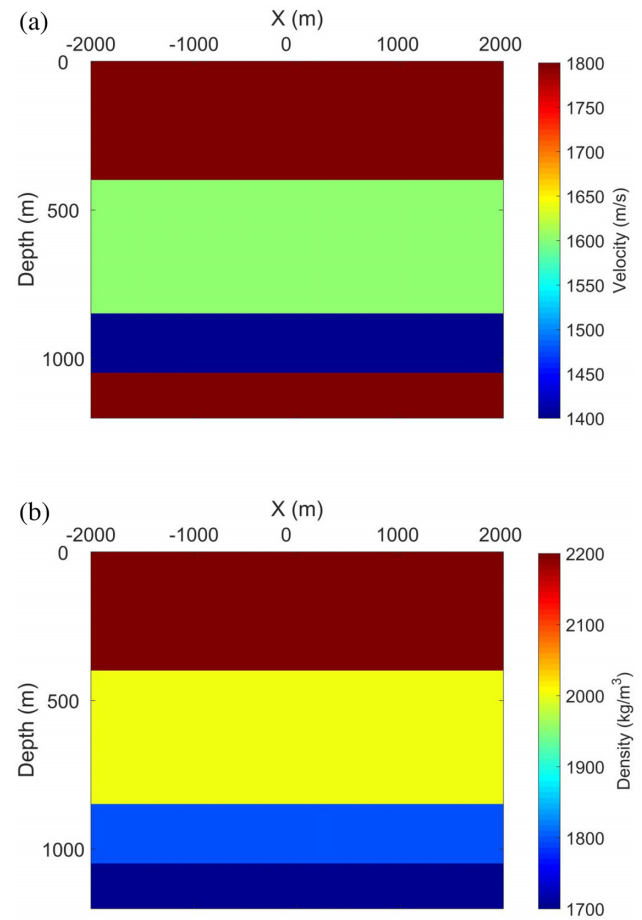

Figure 2. The (a) velocity and (b) density values of the horizontally layered model.

be retrieved with iteration number $k_{max} = 2$ for each time instant t_2. Then eq. (3) is used to retrieve the transmission compensated primary reflections R_r. One of the retrieved data sets is shown in Fig. 3(b). Fig. 3(c) shows the modelled primary reflections without transmission losses, which will be used as a reference to validate the success of our scheme for compensating the transmission losses in
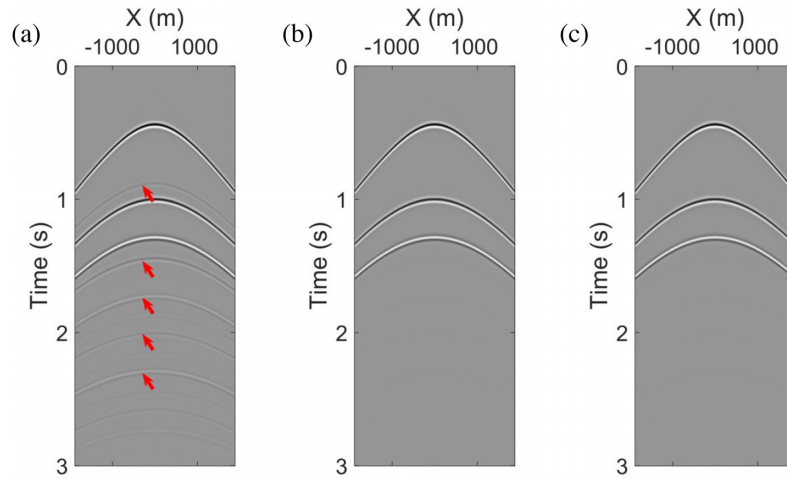
Figure 6. The (a) velocity and (b) density values of the complex medium model.

Figure 7. (a) The modelled reflection response with source at 0 m. The corresponding retrieved data sets by the conventional implementation with $k_{max} = 10$ (b), $k_{max} = 15$ (c) and $k_{max} = 20$ (d), (e) the retrieved data set by the fast implementation and (f) the differences between retrieved gathers by the conventional implementation with $k_{max} = 20$ and fast implementation. The red arrows in (b), (c), (d) and (e) indicate the ghost events. The green arrows in (a), (b) and (c) indicate the multiple reflections and residuals.
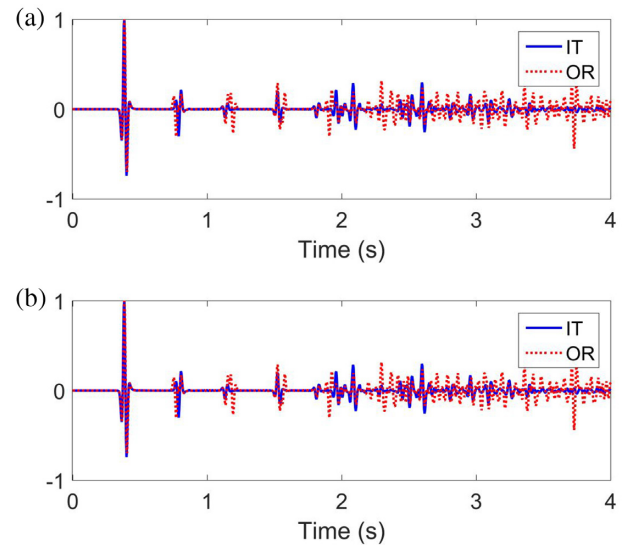
Figure 8. (a) The comparison of zero-offset traces from Figs 7(a) and (d), (b) the comparison of zero-offset traces from Figs 7(a) and (e). OR indicates trace from Fig. 7(a), IT indicates traces from Figs 7(d) and (e).

can be seen that free-surface and internal multiple reflections visible in Fig. 7(a) have been successfully attenuated in Figs 7(b) and (c) and removed in Figs 7(d) and (e). The events indicated by red arrows in Figs 7(b), (c), (d) and (e) are ghost events caused by the presence of diffracted events as analysed by Zhang *et al.* (2019). The green arrows in Figs 7(a), (b) and (c) indicate the multiple reflections and residuals. Fig. 7(f) shows the difference between the resulting gathers retrieved by the conventional implementation with $k_{max} = 20$ and fast implementation with $k_{max} = 2$. It validates the fact that the fast implementation can reduce the computational cost of the proposed scheme by an order of magnitude for retrieving the equivalent result ($k_{max} = 20$ versus $k_{max} = 2$). In order to compare the amplitudes of primary reflections before and after processing, we select zero-offset traces from Figs 7(a), (d) and (e) and show them in Figs 8(a) and (b). It can be seen that multiple reflections have been removed and amplitudes of primary reflections have been changed because of the compensation for transmission losses in both resulting gathers. A similar conclusion can be drawn from Figs 9(a) and (b) where the comparison of nonzero-offset (1000 m) traces from Figs 7(a), (d) and (e) is given. Fig. 10 gives the zero- and non-zero-offset (1000 m) traces from Fig. 7(f). The minor values validate the effectiveness of the fast implementation. The traces in Figs 8–10 have been normalized by the same normalization factor. As analysed by Zhang *et al.* (2019), the transmission losses in the primary reflections are approximately compensated for because the lateral heterogeneity of the complex medium model prevents a full compensation.
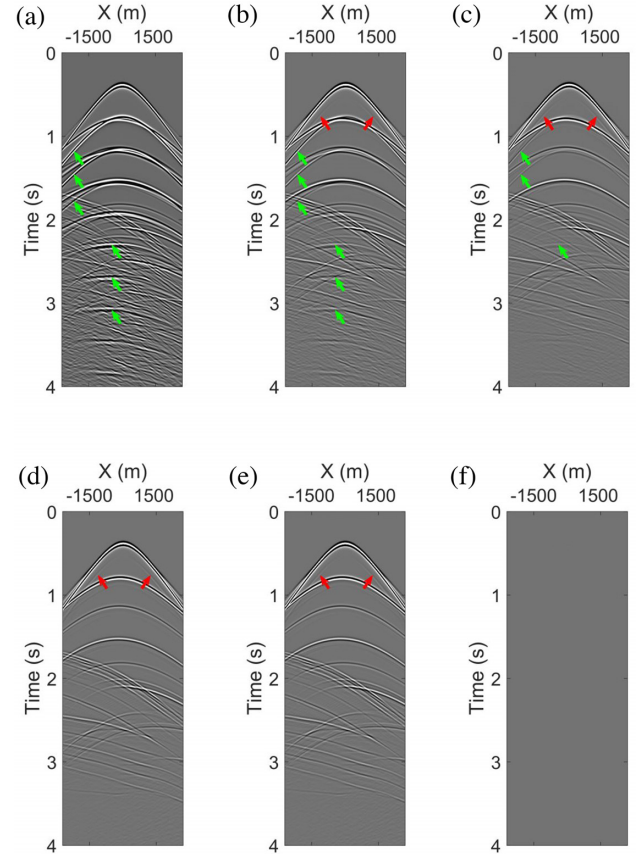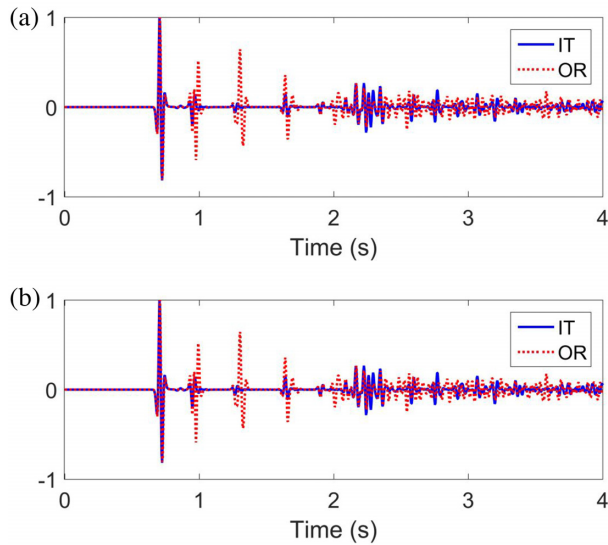
Figure 9. (a) The comparison of non-zero-offset (1000 m) traces from Figs 7(a) and (d), (b) the comparison of non-zero-offset (1000 m) traces from Figs 7(a) and (e). OR indicates trace from Fig. 7(a), IT indicates traces from Figs 7(d) and (e).
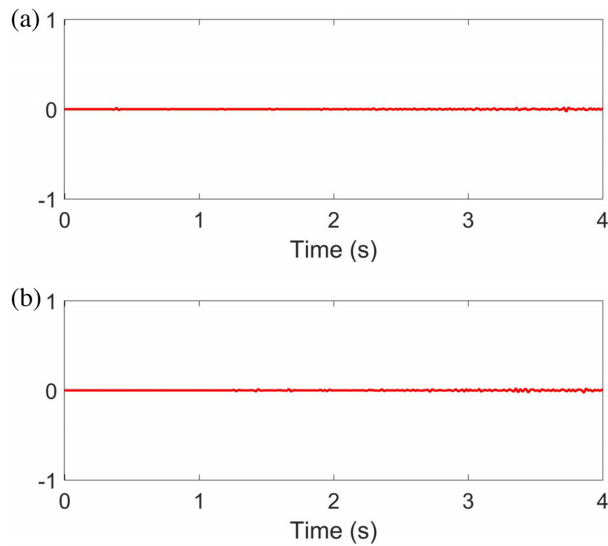

Figure 10. (a) The zero-offset trace from Fig. 7(f) and (b) the non-zero-offset (1000 m) trace from Fig. 7(f).

We use the modelled and retrieved data sets to compute images of the medium. The velocity model shown in Fig. 6(a) is used for the imaging. The images are obtained using a one-way wave equation migration scheme and shown in Fig. 11. The image shown in Fig. 11(a) is from the modelled data set. It contains artefacts arising from free-surface and internal multiple reflections. The images shown in Figs 11(b) and (c) are from the retrieved data set by the conventional implementation with $k_{max} = 20$ and fast implementation. They are free from artefacts arising from free-surface and internal multiple reflections.

LIMITATIONS ANALYSIS

The fast implementation modifies the starting point, but not the operator of the equation which needs to be solved. This means that
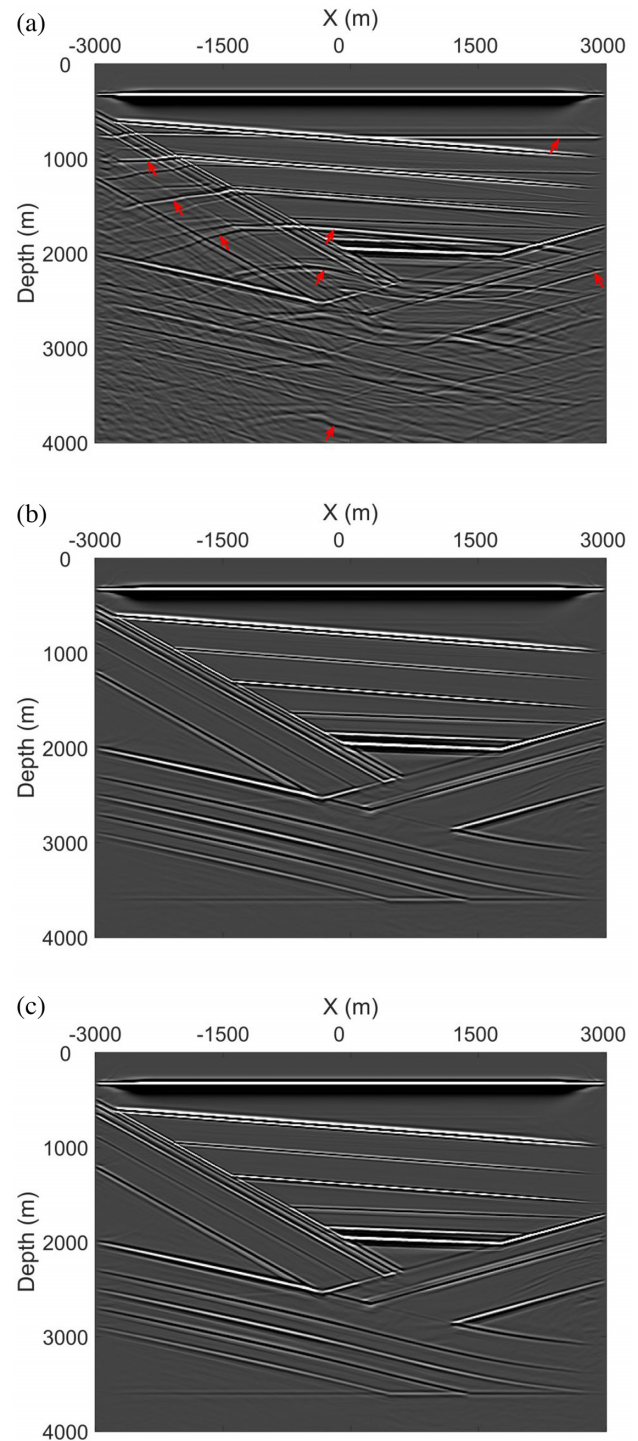
Figure 11. The (a) image retrieved from the modelled reflection responses and (b) the image retrieved from the resulting data set of the conventional implementation with $k_{max} = 20$ and (c) the image retrieved from the resulting data set of the fast implementation. Red arrows in (a) indicate artefacts arising from free-surface and internal multiple reflections.

the same limitations apply to the fast implementation as for the conventional implementation. The limitations have been studied in detail for the convergence properties in Dukalski & de Vos (2018). Because that analysis was done in 1-D, we have carried out some numerical experiments with very high impedance contrasts (leading

to reflection coefficients up to 0.71) and found similar behaviour in 2-D as reported in Dukalski & de Vos (2018).

As shown in the numerical examples section, the fast implementation can reduce the computational cost of the scheme by an order of magnitude. In a field data set, the conventional implementation of the scheme will stop after possibly six or eight iterations because of the imperfect denoising, source signature deconvolution and 3-D compensation. Thus, the fast implementation will not reduce the same amount of computational cost as shown in numerical examples. It will still be much cheaper than the conventional implementation.

Except for these limitations, we have assumed the medium to be lossless and source wavelet to be known. The scheme can also be derived for unknown wavelet (Ravasi 2017; Slob & Wapenaar 2017). A similar scheme as derived here can be derived for a dissipative medium with two-sided reflection and transmission data available (Slob 2016). We further assumed that we can ignore refracted and scattered waves. These assumptions limit the performance of the current scheme. The presented results from the simple and complex 2-D numerical examples show that the proposed scheme has excellent performance in removing free-surface and internal multiple reflections and in compensating for transmission losses in primary reflections when there is no strong reflectors present.

CONCLUSIONS

We have combined the facts that the measured reflection response can act as its own filter to remove free-surface and internal multiple reflections, and to compensate for transmission losses in primary reflections. We have shown that the filters computed for a certain time instant can be used as an initial estimate for the next time instant. This reduces the computational cost in our examples by an order of magnitude. No model information or adaptive subtraction is required. The numerical example in the horizontally layered model shows that the compensation for transmission effects is exact and true reflectivity is retrieved. The complex numerical example shows that the scheme has excellent performance in removing multiple reflections and in compensating for transmission losses. For data sets where the reflections are not too strong, we think this scheme can be of interest in exploration geophysics for retrieving data sets with only transmission compensated primary reflections, velocity model building, artefact-free migration and inversion.

ACKNOWLEDGEMENTS

REFERENCES

Brown, M.P. & Guitton, A., 2005. Least-squares joint imaging of multiples and primaries, *Geophysics,* **70,** S79–S89.

de Melo, F.X., Idris, M., Wu, Z.J. & Kostov, C., 2014. Cascaded internal multiple attenuation with inverse scattering series, in *Proceedings of the 84th Annual International Meeting,* SEG, Expanded Abstracts, pp. 4113–4117.

Dukalski, M. & de Vos, K., 2018. Marchenko inversion in a strong scattering regime including surface-related multiples, *Geophys. J. Int.,* **212,** 760–776.

Löer, K., Curtis, A. & Meles, G.A., 2016. Relating source-receiver interferometry to an inverse-scattering series to derive a new method to estimate internal multiples, *Geophysics,* **81,** Q27–Q40.

Lopez, G. A. & Verschuur, D. J., 2015. Closed-loop surface-related multiple elimination and its application to simultaneous data reconstruction, *Geophysics,* **80,** V189–V199.

Luo, Y., Kelamis, P.G., Huo, S., Sindi, G., Hsu, S. & Weglein, A.B., 2011. Elimination of land internal multiples based on the inverse scattering series, *Leading Edge,* **30,** 884–889.

Matson, K., Corrigan, D., Weglein, A., Young, C. & Carvalho, P., 1999. Inverse scattering internal multiple attenuation: results from complex synthetic and field data examples, in *Proceedings of the 89th Annual International Meeting,* SEG, Expanded Abstracts, 1060–1063.

Meles, G.A., Löer, K., Ravais, M., Curtis, A. & da Costa Filho, C.A., 2015. Internal multiple prediction and removal using Marchenko autofocusing and seismic interferometry, *Geophysics,* **80,** A7–A11.

Ravasi, M., 2017. Rayleigh-Marchenko redatuming for target-oriented, true-amplitude imaging, *Geophysics,* **82,** S439–S452.

Slob, E., Wapenaar, K., Broggini, F. & Snieder, R., 2014. Seismic reflector imaging using internal multiples with Marchenko-type equations, *Geophysics,* **79,** S63–S76.

Slob, E., 2016. Green's function retrieval and Marchenko imaging in a dissipative acoustic medium, *Phys. Rev. Lett.,* **116,** 164301.

Slob, E. & Wapenaar, K., 2017. Theory for Marchenko imaging of marine seismic data with free surface multiple elimination, in *Proceedings of the 79th Conference and Exhibition,* EAGE, Extended Abstracts.

Ten Kroode, P.E., 2002. Prediction of internal multiples, *Wave Motion,* **35,** 315–338.

Thorbecke, J. & Draganov, D., 2011. Finite-difference modeling experiments for seismic interferometry, *Geophysics,* **76,** H1–H18.

van der Neut, J. & Wapenaar, K., 2016. Adaptive overburden elimination with the multidimensional Marchenko equation, *Geophysics,* **81,** T265–T284.

van Groenestijn, G.J.A. & Verschuur, D.J., 2009. Estimating primaries by sparse inversion and application to near-offset data reconstruction, *Geophysics,* **74,** A23–A28.

Verschuur, D., Berkhout, A. & Wapenaar, K., 1992. Adaptive surface-related multiple elimination, *Geophysics,* **57,** 1166–1177.

Wang, Y., Zheng, Y., Zhang, L., Chang, X. & Yao, Z., 2014. Reverse time migration of multiples: eliminating migration artifacts in angle domain common image gathers, *Geophysics,* **79,** S263–S270.

Wang, Y., Zheng, Y., Xue, Q., Chang, X., Fei, T.W. & Luo, Y., 2017. Reverse time migration of multiples: reducing migration artifacts using the wavefield decomposition imaging condition, *Geophysics,* **82,** S307–S314.

Wapenaar, K., Thorbecke, J., van der Neut, J., Broggini, F., Slob, E. & Snieder, R., 2014. Marchenko imaging, *Geophysics,* **79,** WA39–WA57.

Weglein, A.B., Gasparotto, F.A., Carvalho, P.M. & Stolt, R.H., 1997. An inverse scattering series method for attenuating multiples in seismic reflection data, *Geophysics,* **62,** 1975–1989.

Zhang, L. & Slob, E., 2019. Free-surface and internal multiple elimination in one step without adaptive subtraction, *Geophysics,* **84**(1), A7–A11.

Zhang, L., Thorbecke, J., Wapenaar, K. & Slob, E., 2019. Transmission compensated primary reflection retrieval in data domain and consequences for imaging, *Geophysics,* **84**(4), Q27–Q36.